

# An Improved Model of Driving Risk Field for Connected and Automated Vehicles

Ye Tian, Huaxin Pei, Jingxuan Yang, Jianming Hu, Yi Zhang, *Member, IEEE*, and Xin Pei

**Abstract**—Driving risk field is regarded as an effective method to evaluate the driving safety for Connected and Automated Vehicles (CAVs). The existing driving risk field models do not fully consider the impacts of vehicle geometry and vehicle kinematics. So, the performance of the existing models needs to be further improved. In this paper, we establish a more realistic model of the driving risk field. First, vehicle geometry is incorporated into the driving risk field by building an ellipse model to appropriately reflect the vehicle shape. Second, the impacts of different moving directions of vehicles are also considered in the established model to accurately represent vehicle kinematics. Third, we design a computationally efficient function to describe the relations between potential energy and force, which lays a foundation for vehicles to make moving decisions using the driving risk field. Finally, a typical car-following scenario is designed to evaluate the performance of the proposed method with the help of Next Generation Simulation (NGSIM) dataset. Simulation results demonstrate its promising performance in describing traffic safety and driving behavior.

**Index Terms**—Connected and Automated Vehicles, driving risk field, vehicle geometry, car following.

## I. INTRODUCTION

Connected and Automated Vehicles (CAVs) emerges as a promising way to improve traffic safety and efficiency [1], [2]. With the aid of vehicle-to-everything (V2X) technologies, the vehicles can communicate with each other to share the physical attributes and driving states [3]. Based on the abundant traffic information, the driving risk field is proposed to provide a foundation for collision avoidance and trajectory planning [4], which introduces and promotes the concept of “potential field” to mathematically describe the driving risk.

The concept of the driving risk field originated from using the artificial potential field (APF) to plan the trajectory for mobile robots in 1990 [5]. Then, this interesting idea of “potential field” has received widespread attention in making decisions and planning trajectories for mobile robots [6]–[9]. With the development of vehicular technologies and communication technologies, the driving risk field was

This work is supported by Collaboration project between China & Sweden regarding research, development and innovation within life science and road traffic safety under Grant 2018YFE0102800, and National Natural Science Foundation of China under Grant 61673233 and 71671100. (Corresponding author: Yi Zhang)

Y. Tian, H. Pei, and J. Yang are with Department of Automation, Tsinghua University, Beijing 100084, China (e-mail: {y-tian19, phx17, yangjx20}@mails.tsinghua.edu.cn).

J. Hu, Y. Zhang, and X. Pei are with Department of Automation, Beijing National Research Center for Information Science and Technology (BNRist), Tsinghua University, Beijing 100084, China (e-mail: {hujm, zhyi, peixin}@tsinghua.edu.cn).

established for intelligent vehicles. Ni [10]–[12] demonstrated the objectivity and universality of the potential field from the perspectives of both macro and micro, laying the foundation for using the potential field theory in traffic systems. In [13]–[15], a unified driving risk field model of the driver-vehicle-road system is established and verified in the practical applications. On such a basis, Li [16] improved the distribution of driving risk field model to make it more suitable for reality. Chen [17] established a rectangular repulsion and gravitational field around the obstacle vehicle to guide the ego vehicle to achieve obstacle-avoidance trajectory planning. Based on ethical theories, Geisslinger [18] proposed the theory “ethics of risk” and a novel framework for path planning. In [19], [20], the critical parameters of driving states (e.g., acceleration) are introduced into the driving risk field so that each vehicle can predict the driving behaviors of surrounding vehicles more accurately and then plans a safe and efficient trajectory. In [21], [22], the driver’s response was studied and used to comprehensively evaluate the driver’s belief about the probability of a potential accident.

Although many studies have discussed and improved the model of driving risk field for CAVs, there still exist the following major limitations in practical applications. First, the impact of vehicle geometry is ignored when establishing the driving risk field. In most existing studies, the vehicle is regarded as a mass point without considering its physical size. It is inconsistent with the actual driving environment, as vehicle geometry is an important factor affecting driving risk. Second, the way of using the driving risk field in a specific traffic scenario is not clear. The existing studies usually focus on building the model of driving risk field, but the methods of adopting the driving risk field to make moving decisions need to be further studied. Explicit relations between the driving risk model and driving behaviors are always required.

To overcome the above limitations, this paper establishes an improved model of the driving risk field. To make the driving risk field more realistic, the vehicle geometry is considered by building an ellipse model to appropriately describe the vehicle shape, and then the impacts of different moving directions are incorporated in the model to accurately represent vehicle kinematics. To clearly instruct the vehicles how to make decisions using the established model, we design a computationally efficient function to physically describe the relations between potential energy and force.

Theoretical analysis and comparison simulation results jointly demonstrate that the proposed method can better describe the traffic safety and driving behaviors of vehicles.

This paper is organized as follows. *Section II* introduces the concept of the driving risk field. *Section III* proposes an improved model of the driving risk field. *Section IV* evaluates the performance of the proposed model in a car-following scenario by comparing it with typical car-following models. Conclusions and further works are presented in *Section V*.

## II. CONCEPT OF DRIVING RISK FIELD

There exist strong couplings between the trajectories of vehicles in the traffic system. So, the driving behaviors of each vehicle should be adjusted timely according to the motions of its surrounding vehicles to guarantee driving safety. As shown in Fig. 1, *vehicle A* can detect the risk from *vehicle B* and then keep a safe distance from it. *vehicle A* needs to slow down to avoid collision with *vehicle B* when *vehicle A* is close to *vehicle B*. Besides, due to the existence of *vehicle A*, *vehicle B* needs to avoid sudden braking and maintain a certain velocity, so as to avoid collisions with *vehicle A*.

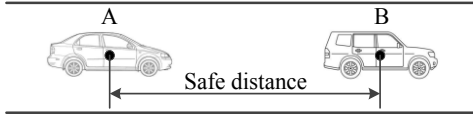


Figure 1. An example of a car-following scenario

Based on the above descriptions, we can find that the driving behaviors and movements of each vehicle could be affected by the surrounding vehicles. According to Newton's first law, "Every object persists in its state of rest or uniform motion in a straight line unless it is compelled to change that state by external force impressed on it" [19]. Therefore, there is no substantial physical touch between vehicles, but we can assume that there is virtual force imposing on the vehicles, so as to change their driving behaviors. This kind of virtual force can be regarded as a field force, as it is determined by the characteristics of vehicle geometry and vehicle kinematics rather than physical contact. The above descriptions indicate that there is a potential field in the traffic system to describe the driving risk between vehicles, namely, the "driving risk field" discussed in this paper.

On this basis, a potential function can be formulated to mathematically describe the degree of driving risk. Similar to Potential theory in Physics, the potential function of the driving risk field has the following characteristics:

- 1) The function value is related to the distance to the surrounding vehicles. The closer to the obstacle vehicle is, the larger the function value and the higher the driving risk are.
- 2) The function value is also related to the characteristics of vehicle geometry and vehicle kinematics of the surrounding vehicles. The larger the size of the vehicle is, the greater the mass and the higher the velocity are, which leads to the larger function value and higher driving risk.

Enabled by V2X, each vehicle can interact with surrounding vehicles and the above information can be obtained in real time. So, the driving risk field model can be established using the obtained traffic information to help the vehicles accurately perceive the potential risks and then lay a foundation for collision avoidance and trajectory planning.

## III. IMPROVED DRIVING RISK FIELD DESIGN

In this section, an improved driving risk field is designed. First, we establish a novel vehicle geometry model to describe the vehicle shape. Then, a complete driving risk field model is established by intergating vehicle geometry and vehicle kinematics. At last, we design a computationally efficient function to describe the relations between potential energy and force, so as to apply the driving risk field in trajectory planning of vehicles.

### A. Vehicle Geometry Model

In this subsection, a new vehicle geometry model is constructed to appropriately describe the shape of vehicles, which is the foundation for building the driving risk field.

In practical applications, vehicle geometry is an important factor that cannot be ignored in evaluating the driving risk, as the larger the size of the vehicle is the greater range of driving risks it generates, which leads to a higher probability of vehicle collisions. In addition, the hit area of vehicles can be approximately represented by a rectangle. When an obstacle collides with the boundary of the rectangle, it is regarded as an accident. Therefore, vehicle geometry cannot be ignored.

Generally, the vehicle shape should be regarded as a rectangle with a definite value of length  $l$  and width  $w$ . However, it suffers high computational complexity in describing driving risk. To improve computational efficiency, we construct an ellipse circumscribed by the rectangle to appropriately describe the vehicle shape, as shown in Fig. 2.

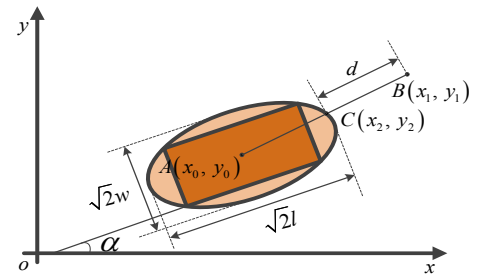


Figure 2. An illustration of using an ellipse to describe vehicle shape.

Taking the longitudinal direction of the road as the  $x$ -axis direction, and the lateral direction as the  $y$ -axis direction. In Fig. 2, we can see that the centroid of the vehicle is at  $(x_0, y_0)$ , and the heading angle of the vehicle is  $\alpha$ . Then, we define the vehicle geometry model as the ellipse circumscribed by the rectangle with the major axis  $\sqrt{2}l$  and the minor axis  $\sqrt{2}w$ . The expression of the vehicle geometry model is

$$\frac{p^2}{l^2} + \frac{q^2}{w^2} = \frac{1}{2}, \quad (1)$$

$$\text{where } \begin{cases} p = (x - x_0) \cos \alpha + (y - y_0) \sin \alpha \\ q = (y - y_0) \cos \alpha + (x - x_0) \sin \alpha \end{cases}$$

As mentioned, the driving risk is highly related to the distance to the obstacle. So, the potential function of driving risk should be constructed by employing the information about the distance to the corresponding vehicle. To this end, in the rest of Section III-A, we will define how to describe the distance  $d$  from a point outside the ellipse to the ellipse.

As shown in Fig. 2, the distance from *point B* to the ellipse refers to the distance from *point B* to *point C*, which is the crossing point with the ellipse on the line connecting *point B* and *point A*. Next, for *point C*, we have

$$\begin{cases} (x_1 - x_0)(y_2 - y_0) = (y_1 - y_0)(x_2 - x_0) \\ \frac{p_2^2}{l^2} + \frac{q_2^2}{w^2} = \frac{1}{2} \end{cases}, \quad (2)$$

where  $\begin{cases} p_2 = (x_2 - x_0) \cos \alpha + (y_2 - y_0) \sin \alpha \\ q_2 = (y_2 - y_0) \cos \alpha + (x_2 - x_0) \sin \alpha \end{cases}$ . By solving (2), the distance between *point A* and *point C* is

$$|AC| = \frac{\sqrt{(x_2 - x_0)^2 + (y_2 - y_0)^2}}{\frac{wl \cdot |AB|}{\sqrt{2w^2 p_1^2 + 2l^2 q_1^2}}}, \quad (3)$$

where  $\begin{cases} p_1 = (x_1 - x_0) \cos \alpha + (y_1 - y_0) \sin \alpha \\ q_1 = (y_1 - y_0) \cos \alpha + (x_1 - x_0) \sin \alpha \end{cases}$ . Obviously, we have

$$d = |AB| - |AC| = |AB| \cdot \frac{\sqrt{2w^2 p_1^2 + 2l^2 q_1^2} - wl}{\sqrt{2w^2 p_1^2 + 2l^2 q_1^2}}. \quad (4)$$

To simplify the calculation, we take the molecule in the upper right corner as the distance parameter, i.e.,

$$d' = \sqrt{2w^2 p_1^2 + 2l^2 q_1^2} - wl. \quad (5)$$

The reason why we can take (5) as a simplified form is that it is an equivalent deformation of (1) and has a certain correlation with the distance to the ellipse. For simplicity, we still use the symbol  $d$  instead of  $d'$  to represent the distance parameter in the following sections.

### B. Driving Risk Field Model

In this subsection, the complete driving risk field model is constructed by considering vehicle geometry and kinematics.

First of all, we need to introduce some parameters to supplement the model. The driving risk is related to the mass and velocity of the vehicle. Generally, the greater the mass and the higher the velocity are, the higher the risk of collision is. Therefore, we introduce a parameter related to the mass and velocity of the vehicle to characterize the driving risk, i.e.,

$$E_i = a_i \cdot m_i v_i^{b_i} + c_i, \quad (6)$$

where  $m_i$  and  $v_i$  are the mass and velocity of the obstacle vehicle, respectively;  $a_i$ ,  $b_i$ , and  $c_i$  are undetermined coefficients;  $a_i, b_i > 0$ .

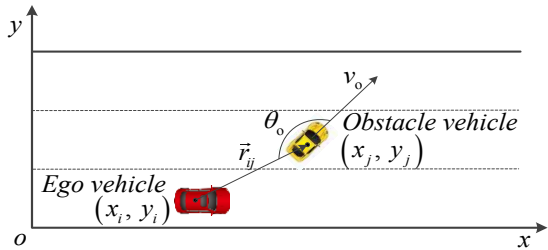


Figure 3. Schematic diagram of the directional difference coefficient

Additionally, driving risk is also affected by the moving directions of vehicles. Specifically, the degree of driving risk in the moving direction of the obstacle vehicle is higher than that of the side and rear. Therefore, it is necessary to introduce the direction inhomogeneous coefficient to accurately describe the impacts of different moving directions. Referring to [14], we correspondingly also use an exponential function to define the direction inhomogeneous coefficient as

$$\xi_{DI} = e^{k_0 v_0 (\cos \theta_0 - 1)}, \quad (7)$$

where  $v_0$  is the velocity of the obstacle vehicle;  $\vec{r}_{ij} = (x_j - x_i, y_j - y_i)$  and  $\theta_0$  is the angle between the

direction of  $v_0$  and  $\vec{r}_{ij}$ ;  $k_0$  is the undetermined coefficient and  $k_0 > 0$ , as shown in Fig. 3.

Equation (7) can describe the law of the driving risk caused by obstacles changing with its velocity and different directions. Specifically, at the same velocity, the smaller  $|\theta_0|$  is, the larger the  $\xi_{DI}$  is, and the higher the driving risk. When  $\theta_0 = 0$ , that is, when the ego vehicle appears in front of the obstacle in the direction of its velocity, the driving risk is the highest. At the same angle, the greater the velocity, the higher the driving risk.

Based on the above analysis, it can be summarized that the closer to the obstacle is, the greater the driving risk is. Further, the driving risk increases with the velocity of vehicles. Importantly, from the perspective of Physics, the interaction between vehicles caused by traffic risk is similar to the interaction between particles described by the Yukawa potential [23]. Therefore, we also utilize an exponential function to characterize the driving risk, and the complete potential function of the driving risk field is defined as

$$V_p = \begin{cases} \lambda \xi_{DI} \cdot E_i \cdot \exp(-k_r \sqrt{d}), & d \geq 0 \\ \lambda E_i, & d < 0 \end{cases}, \quad (8)$$

where  $k_r$  is the steepness coefficient and  $k_r > 0$ , which can determine the steepness of the potential function;  $\lambda$  is the undetermined coefficient and  $\lambda > 0$ .

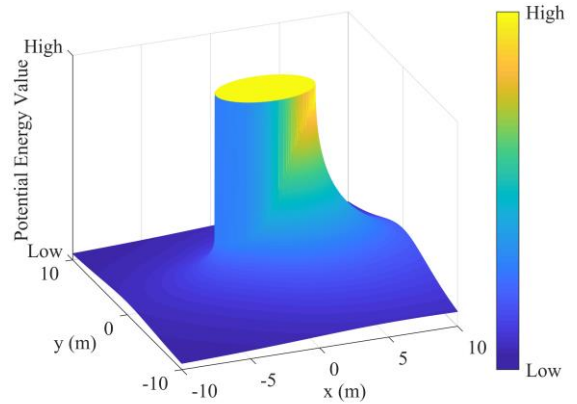


Figure 4. Three-dimensional diagram of the driving risk field.

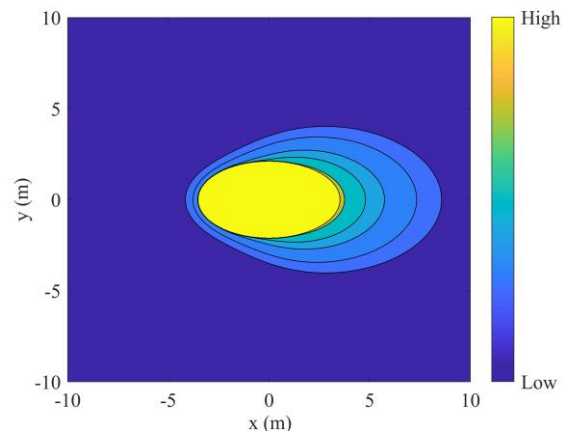


Figure 5. Contour plot of the driving risk field.

Fig. 4 and Fig. 5 are the three-dimensional diagram and contour plot of the driving risk field generated by an obstacle vehicle, respectively. The obstacle vehicle is located at (0, 0) and moving in the  $x$ -direction. From Fig. 4 and Fig. 5, we can see that a potential barrier is formed in the elliptical area around the vehicle, which is determined by the vehicle geometry. The potential energy value inside the ellipse is much higher than the outside, and the potential energy value increases rapidly as the distance from the ellipse reduces, i.e., the driving risk inside the ellipse is much higher than the outside.

TABLE I. VEHICLE ATTRIBUTES AND MOTION STATES SETTINGS

Vehicle	$l$ (m)	$w$ (m)	Location	$v$ (m/s)	$\alpha$ ( $^\circ$ )	$m$ (kg)
A	4	2	(-20, -5)	-8	0	1800
B	5	3	(0, 0)	10	-30	2000
C	6	3	(20, 5)	9	0	2000

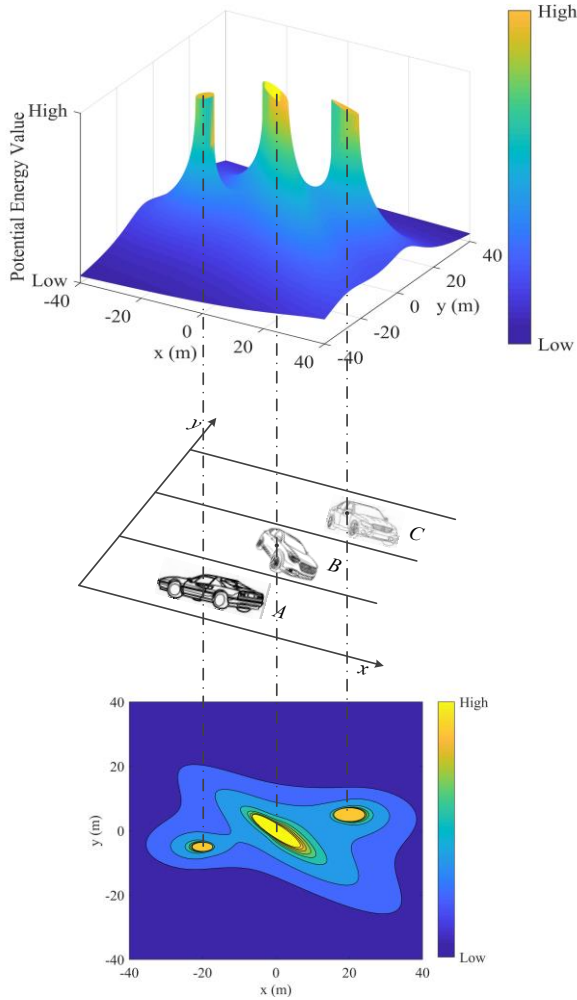


Figure 6. Schematic diagram of the complete driving risk field.

Instead of using a mass point to describe the vehicle geometry as in [13]–[17], [19]–[21], [24], we build an elliptical model in this paper. Fig. 4 and Fig. 5 demonstrate that the proposed driving risk model can characterize driving risk more accurately after considering vehicle geometry. Besides, we can also find that the potential energy value in the

forward direction of the vehicle (i.e., the positive direction of the  $x$ -axis) drops slower than that in the rear. In other words, the driving risk in the front is higher than that in the rear, which is obviously in line with reality. Therefore, the direction inhomogeneous coefficient proposed in this paper is effective and reasonable.

The driving risk field should be the result of superposition when there are multiple obstacles on the road. Obviously, the potential energy superposition law is scalar superposition, as the potential energy is a scalar, i.e.,

$$V_s = \sum_{i=1}^n V_i, \quad (9)$$

where  $V_i$  is the potential energy generated by each obstacle respectively;  $V_s$  is the total potential energy generated by all obstacles;  $n$  is the number of obstacles. To intuitively present the effects of superposition, we design a complex driving scenario with three vehicles to further, as shown in Fig. 6. The attributes and driving states of each vehicle are in TABLE I, and the distribution of the driving risk field is shown in Fig. 6.

We can see that the driving risk field is composed of the field generated by three vehicles at this point. Each vehicle can calculate the potential energy value by (8) efficiently to accurately evaluate the driving risk at each position on the road through the distribution map. On this basis, each vehicle can schedule its driving behaviors to stay away from the high-risk areas to enhance driving safety and improve traffic efficiency.

### C. Application Function

In this subsection, we design a computationally efficient function to describe the relations between potential energy and force, laying a foundation for vehicles to make moving decisions using the driving risk field.

As mentioned in Section II, a vehicle moving on the road will be acted upon by a kind of virtual force. Then, the ego vehicle will stay away from the obstacle and choose a low-risk area to approach. Therefore, this force is generated by the obstacle, and the direction of such force is from the obstacle to the ego vehicle.

The established driving risk field model (8) is described in the form of a potential energy function. We can select the infinity of the road as the zero point of potential energy. Then, according to the relations between the potential energy and the force, the force imposed on the ego vehicle from the driving risk field of the obstacle vehicle can be determined. It consists of the two components in both  $x$  and  $y$  directions. More details about the functions, which describe the relations between potential energy and force, are presented as follows.

The component force in the  $x$ -direction can be defined as

$$\begin{aligned} F_x &= -\frac{\partial V_p}{\partial x} \\ &= k_r \xi_{DI} E_i \cdot \exp(-k_r \sqrt{d}) \cdot \frac{1}{2\sqrt{d}} \cdot \frac{\partial d}{\partial x} \\ &= k_r \xi_{DI} E_i \cdot \exp(-k_r \sqrt{d}) \cdot \frac{w^2 p \cos \alpha + l^2 q \sin \alpha}{(d + wl)\sqrt{d}} \end{aligned} \quad (10)$$

Similarly, the component force in the  $y$ -direction is

$$F_y = k_r \xi_{DI} E_i \cdot \exp(-k_r \sqrt{d}) \cdot \frac{w^2 p \sin \alpha + l^2 q \cos \alpha}{(d + wl)\sqrt{d}}. \quad (11)$$

Then, the magnitude and direction of the resultant force are

$$\left\{ \begin{aligned} |\mathbf{F}| &= \sqrt{F_x^2 + F_y^2} = k_r \zeta_{DI} E_i \cdot \exp(-k_r \sqrt{d}) \\ &\quad \cdot \frac{\sqrt{w^4 p^2 + l^4 q^2 + 4pqw^2 l^2 \sin \alpha \cos \alpha}}{(d + wl)\sqrt{d}} \\ \angle \mathbf{F} &= \arctan\left(\frac{F_y}{F_x}\right) = \arctan\left[\frac{w^2 p \sin \alpha + l^2 q \cos \alpha}{w^2 p \cos \alpha + l^2 q \sin \alpha}\right] \end{aligned} \right. \quad (12)$$

Obviously, the field force superposition law is vector superposition, as the field force has the size and direction, i.e.,

$$\mathbf{F}_S = \sum_{i=1}^n \mathbf{F}_i, \quad (13)$$

where  $F_i$  is the field force generated by each obstacle respectively;  $F_S$  is the total force generated by all obstacles;  $n$  is the number of obstacles. To illustrate the superposition law of field force, we design a typical driving scenario with multiple vehicles, where one vehicle (i.e., *vehicle D*) enters the scenario shown in Fig. 6. The superimposed force imposed on *vehicle D* is shown in Fig. 7.

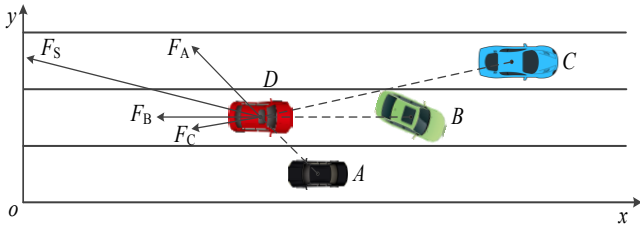


Figure 7. Schematic diagram of the field force superposition.

From Fig. 7, we can see that the resultant force imposed on *vehicle D* is composed of various component forces through vector superposition. In the model of driving risk field, the field force  $F$  can effectively characterize the degree of driving risk. Therefore, the vehicle can timely calculate the force in each direction and then judge the surrounding driving risk in practical applications, so as to schedule its driving behaviors safely and efficiently.

#### IV. SIMULATION RESULTS

In this section, we design a typical car-following scenario to verify the performance of the driving risk field model in describing traffic safety and driving behaviors. Specifically, the improved model of driving risk field is utilized to describe the driving risk encountered by the following vehicle and schedule its driving behavior. Then, we analyze the error between the simulated and the real trajectory data of the following vehicle with help of the NGSIM dataset to demonstrate the effectiveness of the proposed methods.

##### A. Simulation Settings

In the car-following scenario, the following vehicle can obtain real-time driving states of the preceding vehicle and then change its driving behavior according to the field force.

First, we introduce the method of how to calculate the acceleration rate of the following vehicle using the proposed driving risk field model. According to Newton's law, the force leads to the change of the particle's motion state. Correspondingly, the vehicle's motion state changes with the field force during driving. The field force generated by obstacles is a repulsive force in nature. However, in the car-following scenario, the following vehicle always tries to

keep up with the preceding vehicle, i.e., it will also be acted on by a virtual "attractive force" from the preceding vehicle. The magnitude of the attractive force is related to the distance between the two vehicles. When they are far apart, the magnitude is greater, so it will accelerate to catch up with the preceding vehicle; when the distance is short, the magnitude will get smaller accordingly, which is opposite to the repulsive force generated by obstacles. Based on the above analysis, we found that the maximum of the vehicle's acceleration can be combined with the properties of the hyperbolic tangent function to define the expression of the attractive force, which is shown as

$$F_A = a_{\max} \tanh(\mu d), \quad (14)$$

where  $a_{\max}$  is the maximum of the vehicle's acceleration;  $\mu$  is the undetermined coefficient;  $\mu > 0$ . Therefore, in the car-following scenario, the total force acted on by the following vehicle can be shown as

$$F_T = F_A - F_S. \quad (15)$$

According to the fact that the acceleration of a particle motion is proportional to the external force acting on the particle, similarly, we define the acceleration generated by the vehicle under the action of the total force at each moment as

$$a = \frac{F_T}{ame^{\beta v}}, \quad (16)$$

where  $a$  is the acceleration of the vehicle;  $m$  is the mass of the vehicle;  $\alpha$  and  $\beta$  are undetermined coefficients and  $\alpha \neq 0$ .

Then, the popular NGSIM dataset is used to calibrate the improved driving risk field model. This dataset is from US Federal Highway Administration and collected in the United States, which provided the precise location of each vehicle within the study area every 0.1s [25], which can effectively reflect the driver's behavior when facing risks. We filter the car-following pairs from the original dataset on Peachtree Street. The movements of both the following vehicle and leading vehicle can be extracted.

In order to better verify the effectiveness of our proposed model, the same data are also applied to calibrate the parameters of OVM, IDM for comparison, which are two typical car-following models [26], [27].

To evaluate the difference between the simulated results and the real trajectory data in NGSIM, we select the mean absolute percentage error (MAPE) and root mean squares error (RMSE) as the performance metrics in this simulation, i.e.,

$$\text{RMSE} = \sqrt{\frac{\sum_{i=1}^N |x_i^{\text{real}} - x_i^{\text{sim}}|^2}{N}} \quad (17)$$

$$\text{MAPE} = \frac{100}{N} \sum_{i=1}^N \frac{|x_i^{\text{real}} - x_i^{\text{sim}}|}{x_i^{\text{real}}} \quad (18)$$

where  $N$  is the sample size calibrated for the model.  $x_i^{\text{real}}$  is the real value of the data.  $x_i^{\text{sim}}$  is the estimated value simulated by the car-following model.

##### B. Model Calibration

In this simulation, we use the Particle Swarm Optimization (PSO) Algorithm to calibrate the model

parameters, which is a bionic optimization algorithm based on multiple agents [28]. The PSO algorithm has the fast convergence speed and high efficiency so that it is suitable for dataset processing. Therefore, we select the PSO algorithm to calibrate the parameters of the established model in this paper. The calibration results are shown in the TABLE II.

TABLE II. RESULTS OF PARAMETER CALIBRATION

Parameter	Values	Parameter	Values
$\lambda$	1.7831	$c_i$	0.9333
$k_r$	2.0071	$a_{max}$	20.0385
$k_0$	0.0797	$\mu$	2.1867
$a_i$	2.4291	$\alpha$	0.3107
$b_i$	0.0747	$\beta$	0.1412

### C. Performance Evaluation under Car-following Scenario

Taking the car-following pair No.85 & No.89 in NGSIM as an example, the real and simulated trajectories of the following vehicle are shown in Fig. 8. The blue line is the real trajectory of the leading vehicle (No.85). The red line is the real trajectory of the following vehicle (No.89), and the green dotted line is the simulated trajectory of the following vehicle (No.89). Fig. 9 shows the real and simulated velocity of the following vehicle (No.89).

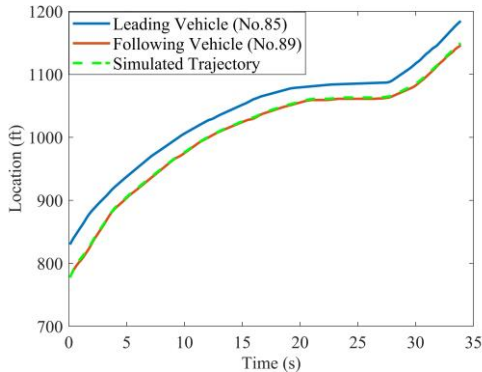


Figure 8. The real and simulated trajectories of vehicle 89.

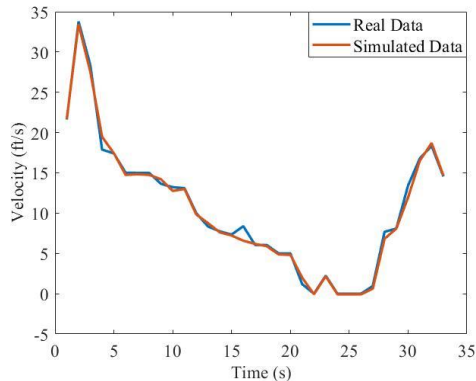


Figure 9. The real and simulated velocity of vehicle 89.

From Fig. 8 and Fig. 9, we can find that the selected car-following pair is a very typical car-following scenario, as it contains the state of deceleration, parking, and start-up

acceleration. Importantly, the simulated trajectory and velocity based on the driving risk field can maintain a small error with the real data, and there is no abnormal phenomenon such as reversing and overtaking.

To further validate the promising performance of the proposed method, the same dataset and PSO algorithm are applied to calibrate the parameters of OVM and IDM for comparison. The simulation results are shown in TABLE III.

TABLE III. COMPARISON RESULTS OF DIFFERENT STRATEGIES

Model	RMSE	MAPE
IDM	3.7245	0.3108
OVM	3.1073	0.2798
Driving risk field	1.8292	0.2075

From the results in TABLE III, it can be found that the model of the improved driving risk field has the smallest error and shows better accuracy than the other two methods. The reasons for this performance can be summarized as follows. Under the environment of CAVs, based on the real-time data communication between vehicles, the proposed model can better describe the driving risk of each vehicle and then help the vehicle to adjust its driving behavior. However, the traditional methods cannot obtain concrete information of vehicle geometry and vehicle kinematics, so that they have a poor performance in describing vehicle behaviors.

## V. CONCLUSION

In this paper, an improved model of the driving risk field is proposed for CAVs for the evaluation of driving safety. The proposed model fully considers the vehicle geometry to accurately evaluate the driving risk of vehicles. Meanwhile, we build a potential energy barrier around the vehicle, establish a potential energy function, and introduce the critical parameters such as the direction inhomogeneous coefficient to make the model more realistic. A computationally efficient function is defined to describe the relations between potential energy and force, which lays a foundation for vehicles to make moving decisions using the driving risk field. Comparison simulation results show that the proposed methods can better describe the driving risk and driving behaviors of vehicles. In the near future, comprehensive decision-making and trajectory planning algorithms will be developed based on the proposed method.

## REFERENCES

- [1] Z. Zhang, Y. Zhang, and D. Yao, "Vehicle-infrastructure cooperation system and auto-pilot: the traffic system presents a comprehensive intelligent trend," *Frontier Science*, vol. 1, no. 2, pp. 56–60, Feb. 2019.
- [2] H. Pei, S. Feng, Y. Zhang and D. Yao, "A cooperative driving strategy for merging at on-ramps based on dynamic programming," *IEEE Transactions on Vehicular Technology*, vol. 68, no. 12, pp. 11646-11656, Dec. 2019.
- [3] H. Pei, Y. Zhang, Q. Tao, S. Feng and L. Li, "Distributed cooperative driving in multi-intersection road networks," *IEEE Transactions on Vehicular Technology*, doi: 10.1109/TVT.2021.3079272.
- [4] Y. Tian, H. X. Pei, Y. Zhang, "A strategy for making lane-change decision based on improved driving risk field and BP neural network,"

- in *5th International Conference on Electronic Information Technology and Computer Engineering*, Xiamen, China, 2020, pp. 669–675.
- [5] O. Khatib, "Real-time obstacle avoidance for manipulators and mobile robots," in *Autonomous Robot Vehicles*, I. J. Cox and G. T. Wilfong, Eds. New York, NY: Springer New York, 1990, pp. 396–404.
  - [6] Z. Pan, D. Li, and K. Yang, "Multi-robot obstacle avoidance based on the improved artificial potential field and PID adaptive tracking Control Algorithm" *Robotica*, vol. 37, no. 11, pp. 1883–1903, Apr. 2019.
  - [7] U. Orozco-Rosas, O. Montiel, and R. Sepúlveda, "Mobile robot path planning using membrane evolutionary artificial potential field," *Applied Soft Computing*, vol. 77, pp. 236–251, Jan. 2019.
  - [8] P. B. Kumar, H. Rawat, D. R. Parhi, "Path planning of humanoids based on artificial potential field method in unknown environments," *Expert Systems*, vol. 36, no. 2, pp. 1–12, Dec. 2018.
  - [9] A. Azzabi, K. Nouri, "An advanced potential field method proposed for mobile robot path planning," *Transactions of the Institute of Measurement and Control*, vol. 41, no. 11, pp. 3132–3144, Jul. 2019.
  - [10] D. Ni, "A unified perspective on traffic flow theory. Part I: the field theory," *Applied Mathematical Sciences*, vol. 7, no. 39, pp. 1929–1946, Nov. 2012.
  - [11] D. Ni, "A unified perspective on traffic flow theory. Part II: the unified diagram," *Applied Mathematical Sciences*, vol. 7, no. 37–40, pp. 1947–1963, Nov. 2012.
  - [12] D. Ni, "A unified perspective on traffic flow theory. Part III: validation and benchmarking," *Applied Mathematical Sciences*, vol. 7, no. 40, pp. 1965–1982, Nov. 2012.
  - [13] J. Wang, J. Wu, Y. Li, and K. Li, "The concept and modeling of driving safety field based on driver-vehicle-road interactions," in *17th International IEEE Conference on Intelligent Transportation Systems (ITSC 2014)*, Qingdao, China, 2014, pp. 974–981.
  - [14] J. Wang, J. Wu, X. Zheng, D. Ni, and K. Li, "Driving safety field theory modeling and its application in pre-collision warning system," *Transportation Research Part C: Emerging Technologies*, vol. 72, pp. 306–324, Oct. 2016.
  - [15] J. Wang, J. Wu, and Y. Li, "Driving safety field based on driver-vehicle-road interactions," *IEEE Transactions on Intelligent Transportation Systems*, vol. 16, no. 4, pp. 2203–2214, Aug. 2015.
  - [16] M. Li, X. Song, H. Cao, J. Wang, Y. Huang, C. Hu, and H. Wang, "Shared control with a novel dynamic authority allocation strategy based on game theory and driving safety field," *Mechanical Systems and Signal Processing*, vol. 124, no. 1, pp. 199–216, Jun. 2016.
  - [17] H. Chen, C. Shen, H. Guo, and J. Liu, "Moving horizon path planning for intelligent vehicle considering dynamic obstacle avoidance," *China Journal of Highway and Transport*, vol. 32, no. 1, pp. 166–176, Jan. 2019.
  - [18] M. Geisslinger, F. Poszler, J. Betz, C. Lütge, and M. Lienkamp, "Autonomous driving ethics: from trolley problem to ethics of risk," *Philos. Technol*, Apr. 2021, doi: 10.1007/s13347-021-00449-4.
  - [19] L. Li, J. Gan, X. Qu, P. Mao, and B. Ran, "Car-following model based on safety potential field theory under connected and automated vehicle environment," *China Journal of Highway and Transport*, vol. 32, no. 12, pp. 76–87, Dec. 2019.
  - [20] L. Li, J. Gan, X. Ji, X. Qu, and B. Ran, "Dynamic driving risk potential field model under the connected and automated vehicles environment and its application in car-following modeling (Periodical style—Accepted for publication)," *IEEE Transactions on Intelligent Transportation Systems*, to be published.
  - [21] Dunning, A. Ghoreyshi, M. Bertucco, and T. D. Sanger, "The tuning of human motor response to risk in a dynamic environment task," *PLoS ONE*, vol. 10, no. 4, p. e0125461, Apr. 2015, doi: 10.1371/journal.pone.0125461.
  - [22] S. Kolekar, J. de Winter, and D. Abbink, "Human-like driving behaviour emerges from a risk-based driver model," *Nat Commun*, vol. 11, no. 1, Sep. 2020, doi: 10.1038/s41467-020-18353-4.
  - [23] S. A. Khrapak, A. V. Ivlev, G. E. Morfill, S. K. Zhdanov and H. M. Thomas, "Scattering in the attractive Yukawa potential: application to the ion-drag force in complex plasmas," *IEEE Transactions on Plasma Science*, vol. 32, no. 2, pp. 555–560, Apr. 2004.
  - [24] A. Pierson, W. Schwarting, S. Karaman, and D. Rus, "Navigating congested environments with risk level sets," in *2018 IEEE International Conference on Robotics and Automation (ICRA 2018)*, Brisbane, Australia, 2018, pp. 5712–5719.
  - [25] Z. Chen and B. B. Park, "Preceding vehicle identification for cooperative adaptive cruise control platoon forming," *IEEE Transactions on Intelligent Transportation Systems*, vol. 21, no. 1, pp. 308–320, Jan. 2020.
  - [26] M. Bando, K. Hasebe, A. Nakayama, A. Shibata, and Y. Sugiyama, "Dynamical model of traffic congestion and numerical simulation," *Physical Review E*, vol. 55, no. 2, pp. 1035–1042, Feb. 1995.
  - [27] M. Treiber, A. Hennecke, and D. Helbing, "Congested Traffic States in Empirical Observations and Microscopic Simulations," *Physical Review E*, vol. 62, no. 2, pp. 1805–1824, Aug. 2000.
  - [28] J. H. Lee, J. Kim, J. Song, Y. Kim and S. Jung, "A novel memetic algorithm using modified particle swarm optimization and mesh adaptive direct search for PMSM design," *IEEE Transactions on Magnetics*, vol. 52, no. 3, pp. 1–4, Mar. 2016.